Kinetochore-independent mechanisms of sister chromosome separation

Hannah Vicars[1], Travis Karg[1], Brandt Warecki[1], Ian Bast[1], William Sullivan[1]*.

[1] Department of Molecular, Cell and Developmental Biology, University of California, Santa Cruz, Santa Cruz, CA, USA

*Email: wtsulliv@ucsc.edu (WS)

Author contributions: HV contributed to all aspects of planning, execution of the experiments, analysis, and manuscript preparation. TK contributed to the planning, execution, and analysis of the RNAi screen and the planning and execution of live imaging of Greatwall hypomorphs. BW contributed to the planning, execution, and analysis of the telomere-labeling experiments. IB contributed to the execution and analysis of the telomere-labeling experiments. WS contributed to all aspects of experimental planning and manuscript preparation.

ABSTRACT

Although kinetochores normally play a key role in sister chromatid separation and segregation, chromosome fragments lacking kinetochores (acentrics) can in some cases separate and segregate successfully. In *Drosophila* neuroblasts, acentric chromosomes undergo delayed, but otherwise normal sister separation, revealing the existence of kinetochore-independent mechanisms driving sister chromosome separation. Bulk cohesin removal from the acentric is not delayed, suggesting factors other than cohesin are responsible for the delay in acentric sister separation. In contrast to intact kinetochore-bearing chromosomes, we discovered that acentrics align parallel as well as perpendicular to the mitotic spindle. In addition, sister acentrics undergo unconventional patterns of separation. For example, rather than the simultaneous separation of sisters, acentrics oriented parallel to the spindle often slide past one another toward opposing poles. To identify the mechanisms driving acentric separation, we screened 117 RNAi gene knockdowns for synthetic lethality with acentric chromosome fragments. In addition to well-established DNA repair and checkpoint mutants, this candidate screen identified synthetic lethality with X-chromosome-derived acentric fragments in knockdowns of Greatwall (cell cycle kinase), EB1 (microtubule plus-end tracking protein), and Map205 (microtubule-stabilizing protein). Additional image-based screening revealed that reductions in Topoisomerase II levels disrupted sister acentric separation. Intriguingly, live imaging revealed that knockdowns of EB1, Map205, and Greatwall preferentially disrupted the sliding mode of sister acentric separation. Based on our analysis of EB1 localization and knockdown phenotypes, we propose that in the absence of a kinetochore, microtubule plus-end dynamics provide the force to resolve DNA catenations required for sister separation.

AUTHOR SUMMARY

Kinetochores, the site on the chromosomes to which microtubules attach driving the separation and segregation of replicated sister chromosomes, have been viewed as essential for proper cell division and accurate transmission of chromosomes into daughter cells. However previous studies demonstrated that sister chromosomes lacking kinetochores (acentrics) often undergo separation, segregation and transmission. Here we demonstrate that sister acentrics are held together through DNA intertwining. We show that during anaphase, acentric sister separation is achieved through Topoisomerase activity, an enzyme that resolves these DNA linkages, as well as forces generated on the acentrics by the growing ends of highly dynamic microtubule polymers. We found that acentric sister chromatids display unique patterns of separation using mechanisms independent of the kinetochore. Additionally, we identified the specific microtubule-associated proteins required for the successful mitotic transmission of acentric chromosomes to daughter cells. These studies reveal unsuspected, distinct forces that likely act on all chromosomes during mitosis independent of kinetochore-microtubule attachments.

INTRODUCTION

Eukaryotic cells have evolved mechanisms to detect and protect against genomic insults. These mechanisms include checkpoint pathways that delay cell cycle progression allowing time for repair as well as apoptotic pathways that eliminate the damaged cells from the dividing population [1]. Although a great deal is known regarding the function of these corrective pathways during interphase, much less is known about the mechanisms that protect against genomic instability after exit from metaphase. Studies demonstrate that DNA damage persisting through metaphase delays anaphase onset. This delay is mediated both by the DNA damage and spindle assembly checkpoint pathways [2, 3].

Despite these mechanisms, if the DNA damage remains, the checkpoints are overridden, and the cell exits metaphase [4]. The persistence of unrepaired double-strand breaks (DSBs) at

54 metaphase is particularly problematic due to the formation of chromosome fragments, one of
55 which lacks a telomere and the other lacking a kinetochore and a telomere. The latter type are
56 known as acentrics and are incapable of forming canonical microtubule-kinetochore attachments
57 that drive sister chromosome separation and segregation. Consequently, acentrics would be
58 expected to lag on the metaphase plate and exhibit severe segregation defects. In accord with
59 this expectation, acentrics often fail to segregate, are excluded from daughter nuclei, and
60 subsequently form cytoplasmic micronuclei [5-7]. However, a growing number of reports
61 demonstrate poleward migration of acentric chromosome fragments [5, 8-13]. Proposed
62 mechanisms of acentric segregation include neo-centromere formation [14] and direct
63 association of the acentric chromosome with microtubules [15] or a kinetochore-bearing
64 chromosome [16-18].

65 Acentrics are efficiently induced in *Drosophila* bearing an I-CreI endonuclease
66 transgene, which fortuitously recognizes a repetitive sequence within the pericentric rDNA repeats
67 of the *Drosophila* X chromosome [19-22]. Induction of I-CreI expression results in the formation
68 of acentrics in over 80% of third instar larval neuroblast cells [12]. Although acentrics lag behind
69 on the metaphase plate well after the intact chromosomes migrate toward opposite poles, the
70 acentrics have a remarkable ability to accurately separate, segregate and incorporate into
71 daughter telophase nuclei [23]. A previous study done in the lab found that acentric segregation
72 relies on the chromokinesin Klp3A and interpolar microtubules [15]. However, it remains unclear
73 how sister acentrics are held together on the metaphase plate well after the main chromosome
74 mass has separated. Additionally, it is unknown how acentric sisters are able to initially separate
75 from one another instead of segregating together poleward. These behaviors reveal the existence
76 of kinetochore-independent mechanisms maintaining sister chromosome association on the
77 metaphase plate and driving their separation during anaphase. Possible explanations include
78 delayed acentric cohesin removal, delayed resolution of sister DNA catenations, or opposing plus-
79 end directed microtubule forces acting on each sister. Here we employ a combination of synthetic

80 lethal screens and live imaging to identify factors required for proper separation of sister acentrics.
81 Live analysis reveals three distinct modes of acentric separation: unzipping, sliding, and
82 simultaneous dissociation. This candidate screen revealed that Topoisomerase II, the cell-cycle
83 regulator Greatwall kinase, the microtubule (MT) plus-end tracking protein EB1, and the MT-
84 associated protein Map205 provide key roles in sister separation of acentrics. In addition, gene
85 knockdowns of EB1, Map205, and Greatwall preferentially disrupt the sliding mode of sister
86 separation. As will be discussed, this analysis demonstrates the existence of kinetochore-
87 independent mechanisms facilitating sister chromosome separation.

88 **RESULTS**

89 **Acentric sister separation, but not cohesin removal, is delayed during the metaphase-to-**
90 **anaphase transition**

91 As described previously, acentric chromosome fragments are efficiently generated
92 through heat-shock induction of an I-CreI transgene that specifically targets and creates DSBs in
93 the rDNA repeats at the base of the *Drosophila* X chromosome [19]. In accord with previous
94 studies [12], live analysis of the resulting X chromosome acentrics in the larval neuroblasts
95 reveals that sister separation of the acentrics occurs on average 148 seconds (± 44, N=19) after
96 separation of the intact chromosomes (**Figure 1**). We define acentric sister separation as the
97 point in which the sister acentrics can be clearly distinguished. Acentric sister segregation is
98 defined as the interval between separation of sisters and their migration to the spindle pole. The
99 delay in timing of acentric separation is defined as the time elapsed between the initiation of intact
100 sister chromosome separation and that of acentric sister separation. Sister chromatids are held
101 together at metaphase by cohesin, a tripartite ring-like protein complex comprised of two structural
102 maintenance of chromosome proteins (SMC1, SMC3) and a kleisin subunit (Rad21/Scc1) [24,
103 25]. Initially, cohesin removal occurs only along the chromosome arms through proteolytic
104 cleavage of the kleisin subunit by separase just prior to anaphase onset [26-28]. Due to the

105 Sgo/PP2A-dependent protection mechanism, cohesin remains at the centromeric regions [29].
106 Once cohesin is removed, microtubules drive sister separation [30, 31].

107 **Fig 1: Acentric sister separation is delayed relative to kinetochore-bearing chromosomes**
108 **during anaphase.** (A) Still frames of a time-lapse movie of a mitotic neuroblast labeled with H2Av-RFP
109 and not expressing I-CreI. (B) Still frames of a time-lapse movie of a mitotic neuroblast with I-CreI induced
110 acentrics. Separation of sister acentrics (arrows) is delayed. Consequently, they lag on the spindle equator
111 but eventually separate, segregate, and are reincorporated into daughter nuclei. Bars, 2 μm. Time in
112 seconds. (C) Scatterplot showing the delay in acentric sister separation after anaphase onset. Delay
113 (seconds) was measured from when kinetochore-bearing chromosomes initiated separation to when
114 acentric sister chromosomes initiated separation. Bars represent mean and standard deviations.
115

116 To investigate if delays in cohesin release are responsible for the delayed separation of
117 acentric chromosomes, female neuroblast divisions were live imaged with a cohesin component,
118 Rad21, tagged with EGFP [32]. Time-lapse images of a control neuroblast expressing Rad21-
119 EGFP are shown in **Figure 2A** (chromosomes in magenta, cohesin in green). No lagging
120 chromosomes are observed and Rad21 is cleared off of all chromosomes just prior to anaphase
121 onset and separation of sister chromatids. **Figure 2B** and **Movie S1** show time- lapse images of
122 an I-CreI-expressing neuroblast division. Separation and segregation of sister acentrics is delayed
123 relative to the intact chromosomes. Interestingly, cohesin removal just prior to anaphase onset
124 from the acentrics and the intact kinetochore-bearing chromosomes occurs simultaneously. This
125 is more clearly seen in the single channel black and white cohesin images of **Figure 2B** (depicting
126 yellow outlined regions of **Figure 2B**). Quantification of the Rad21 fluorescent signal supports the
127 conclusion of a relatively synchronous removal of cohesin on the acentric and intact
128 chromosomes (**Figure 2C**). The finding that sister acentrics remain paired despite the absence
129 of cohesin and well after the intact chromosomes have separated, indicate additional forces must
130 hold sister acentrics together.

131 **Fig 2: Cohesin complexes are cleared off of acentric sisters upon anaphase onset.** Chromosomes
132 labeled with H2Av-RFP (magenta) and cohesin labeled with Rad21-EGFP (green). (A) Stills from a time-
133 lapse movie of a control mitotic neuroblast. (B) Still images from a time-lapse movie of a mitotic neuroblast
134 with I-CreI-induced acentrics (Movie S1). Acentrics (arrowhead) lag on the spindle equator. (C) Bar graphs
135 of a compilation of five videos of I-CreI- expressing neuroblasts showing the relative fluorescence intensities
136 in arbitrary units (AU) of chromosomes (H2Av-RFP, top) cohesin (Rad21-EGFP, bottom) around acentrics
137 (cyan outlined region) and the main mass of chromosomes (yellow outlined region) at time points 50, 40,

25, 0 s, prior to anaphase onset, respectively. Bars, 2 μm. Time in seconds. Error bars represent standard deviations of fluorescence intensities at all points tested.

Acentric sister separation occurs via three distinct patterns

To examine dynamics of acentric separation, we imaged live neuroblasts expressing I-CreI, the histone marker H2Av-RFP, and the telomere marker HOAP-GFP [33]. Marked telomeres enabled us to determine the orientation of acentrics with respect to one another as they aligned on the metaphase plate, separated, and segregated poleward [15]. We observed three distinct patterns of sister acentric separation (**Figure 3**). In the most frequent pattern (49%, N=45), acentric pairs separate by sliding past one another (**Figure 3A**, Top row: histone-labeled chromosomes in magenta, HOAP-labeled telomeres in green). This is more clearly observed in the single histone channel movie (**Figure 3A** Bottom row and **Movie S2**). Also, in contrast to intact kinetochore-bearing chromosomes which always align perpendicular to the spindle, the paired sister acentrics align either parallel or perpendicular to the spindle and division axis.

Fig 3: Sister acentrics separate via three distinct patterns. Chromosomes labeled with H2Av-RFP (magenta) and telomeres labeled with HOAP-GFP (green). Telomeres indicated by yellow arrowheads. Direction of separation indicated by white arrows. (A) Top row: Still images of a time-lapse movie of a mitotic neuroblast with I-CreI induced acentrics showing sister acentrics (cyan arrows) lagging behind during anaphase, paired with telomeres opposing, sliding past one another, and ultimately separating. Bottom row: Black and white images of sister acentrics sliding past one another (see arrows) (Movie S2). (B) Top row: Still images of a time-lapse movie of a mitotic neuroblast with I-CreI induced acentrics showing acentrics (cyan arrows) lagging on the metaphase plate. In a process we term “unzipping”, sister acentrics are aligned with telomeres paired, initiate separation at their broken ends followed by separation of telomeres. Bottom row: Black and white images of sister acentrics unzipping (see arrows). (C) Top row: Still images of a time-lapse movie of a mitotic neuroblast with I-CreI induced acentrics showing sister acentrics (cyan arrows) lagging behind during anaphase. In a process we term “simultaneous dissociation”, sister acentrics simultaneously separate along their entire length. Bottom row: Black and white images of sister acentrics simultaneously separating along their entire length (see arrows). (D) Frequency of acentric sisters paired with their telomeres aligned or in opposite orientations. (E) Measurements of the frequency of each mode of acentric sister separation (x-axis) and the timing of acentric sister separation after intact chromosomes separate (y-axis). Each dot represents on acentric pair. Black dots represent acentric sisters with telomeres aligned and purple dots represent acentric sisters with telomeres oriented in opposite directions. Boxes show interquartile ranges and lines show medians of the measured data. Asterisks represent statistical significance (***P=0.0008) determined by Mann-Whitney tests. (F) Chart showing the distribution of telomere orientations within each mode of acentric sister separation. Acentrics that separate by unzipping are always oriented with their telomeres paired.

177 The second pattern of acentric separation occurs via an “unzipping” mechanism (**Figure**
178 **3B**). This pattern occurs at a frequency of 31% (N=45). During separation, sister acentrics often
179 first separate at the broken end followed by separation at the telomere. This is illustrated in **Figure**
180 **3B**: the telomeres remain associated while the broken ends are well separated. Rarely, the paired
181 acentrics unzip from the telomere end first. In contrast to the acentrics that separate by sliding,
182 these paired sister acentrics are frequently aligned perpendicular to the spindle and division axis.
183 In the third pattern of separation, the remaining 20% (N=45), acentric sisters cleanly
184 separate from one another along their entire length similar to that observed for centric
185 chromosomes (**Figure 3C**). We termed this centric-like pattern: simultaneous dissociation.
186 Acentrics that separate via simultaneous dissociation are aligned in multiple orientations on the
187 metaphase plate (from parallel to perpendicular) with respect to the spindle and division axis. At
188 separation, dissociating sister acentrics simultaneously separate along their entire lengths.
189 We next analyzed the orientation of sister acentrics with respect to one another at the time
190 of separation through labeling telomeres with HOAP-GFP. As expected, the vast majority (87%,
191 39/45) of sister acentrics were oriented with their telomeres paired and aligned (**Figure 3D**).
192 However, a small but notable fraction (13%, 6/45), aligned with their telomeres opposed (**Figure**
193 **3D**). Acentric pairs that align with telomeres opposed presumably have already lost catenation
194 and/or cohesin in order to adopt this geometry. 14% and 33% of acentric sisters that separated
195 by sliding and dissociating, respectively, aligned with their telomeres opposed. Interestingly, sister
196 acentrics that separated by unzipping were never observed aligned with their telomeres opposed.
197 This suggests that there is an absolute requirement for sister pairing in acentrics that separate by
198 unzipping.
199 To further characterize these three modes of acentric separation, we measured the time
200 from anaphase onset (as determined by separation of the intact chromosomes) to sister acentric
201 separation (**Figure 3E**). Sliding acentrics separated much later than acentrics (202 ± 51 seconds)
202 that separated either by unzipping (131 ± 54 seconds) or dissociating (106 ± 55 seconds) (N=45,

203 **Figure 3E**). These differences were statistically significant as determined by two-sided Mann-
204 Whitney tests (P=0.0008 and P=0.0008, respectively). We did not detect any difference in the
205 timing of acentric sister separation by unzipping or dissociating (P=0.25 as determined by a two-
206 sided Mann-Whitney test).

207 Taken together, these results demonstrate three distinct patterns for acentric separation.
208 We note that based on the movements and orientation of both sliding and dissociating acentrics,
209 it is possible that catenations are lost along the entire length of the acentric pair simultaneously
210 at the moment of separation. In contrast, acentrics that separate by unzipping and appear to have
211 an absolute requirement for sister pairing may be more tightly associated with one another, and
212 this tight association may be due to lingering catenations.

213 **Synthetic lethal screen identifies genes required for separation of sister acentrics**

214 To identify the mechanisms required for transmission of acentric sister chromosomes, we
215 screened candidate RNAi gene knockdowns that resulted in synthetic lethality in the presence of
216 acentrics. The rationale for this screen is based on previous studies demonstrating that I-CreI
217 induction of acentric chromosomes during third instar larval stage resulted in only slight reductions
218 in adult survival because the acentrics are efficiently transmitted to daughter nuclei [12]. However,
219 reducing or partially disrupting the function of genes required for the normal acentric transmission
220 results in a dramatic reduction in adult survival upon acentric induction [12, 15]. Thus, we
221 expected that a subset of the gene knockdowns that resulted in synthetic lethality upon I-CreI
222 induction would be required for proper pairing and segregation of sister acentrics.

223 To perform the screen, adult flies bearing a heat-shock inducible I-CreI endonuclease and
224 Gal4 under the control of a ubiquitously expressed Actin enhancer element (Act5) were crossed
225 to adults bearing UAS-gene specific RNAi constructs. Lethality of heat-shocked (I-CreI induced)
226 and non-heat-shocked (I-CreI not induced) F1 progeny bearing both constructs were assayed.
227 RNAi constructs that significantly increased lethality upon I-CreI induction were of particular
228 interest. We screened 117 candidate genes for synthetic lethality upon acentric induction

229 (**Table S1**). These included genes encoding proteins spanning a diversity of mitotic
230 functions, including microtubule-associated proteins, chromatin remodelers, DNA repair genes,
231 cell cycle kinases, and cell cycle checkpoints. For each RNAi line, we determined the survival
232 ratio of the RNAi knockdown with I-CreI induced to the RNAi knockdown alone (RNAi knockdown
233 + I-CreI/RNAi knockdown) (**Table 1**). Because these RNAi knockdowns do not cause complete
234 lethality, we classified hits as having a survival ratio of 65% or less (**Table 1**).

	Gene RNAi	Survival rate with RNAi and I-CreI induced / Only RNAi induced	Rate of larvae-to-adult survival of RNAi with I-CreI induction % ± SD (N)	Rate of larvae-to-adult survival of RNAi without I-CreI induction % ± SD (N)	Gene function
	Wildtype (Control)		80 ± 21 (194)	91 ± 7 (194)	—
Chromatin-associated:	*hyx* (2)	10%	8 (25)	88 (25)	Transcription factor
	cap-D2	12%	6 (17)	50 (12)	Condensin
	chd1	30%	10 ± 17 (69)	33 ± 6 (99)	ATP-dependent chromatin remodeling
	sin3A	33%	8 (25)	24 (25)	Histone deacetylase, transcription regulator
	chrac-14 (2)	48%	48 (25)	100 (25)	Nucleosome mobilization, chromatin assembly
	chd1 (2)	50%	48 (25)	95 (23)	ATP-dependent chromatin remodeling
	spt4	55%	24 (25)	44 (25)	Transcription elongation factor
	sir2	60%	64 (25)	94 (16)	Histone deacetylase, heterochromatin gene silencing
	hp1e	65%	65 (20)	100 (25)	Heterochromatin protein 1 (chromosome segregation)
Microtubule-associated:	*msps*	27%	18 ± 17 (56)	67 ± 24 (30)	Mitotic spindle, microtubule nucleation
	asp (2)	46%	44 (25)	96 (25)	Astral microtubule organization, spindle orientation
	EB1	47%	44 ± 25 (86)	94 ± 9 (38)	Microtubule plus-end binding, chromosome segregation
	Klp68D	51%	29 (24)	57 (21)	Kinesin motor protein, microtubule-based transport
	asp	52%	52 (25)	100 (15)	Astral microtubule organization, spindle orientation
	map205	65%	54 ± 18 (141)	83 ± 13 (91)	Binds/stabilizes microtubules
DNA repair/ checkpoint:	*spnA*	2%	2 ± 4 (57)	82 ± 18 (99)	Rad51 double-strand break repair
	mus309	11%	10 ± 1 (42)	95 (22)	Double-strand break repair
	ku80	29%	28 (25)	96 (25)	Non-homologous end joining double-strand break repair
	tefu	43%	43 (30)	100 (25)	DNA damage checkpoint
	cp190	48%	12 (17)	25 (12)	Chromatin silencing, DNA damage response
Cell cycle kinase:	*bubR1*	3%	1 ± 2 (168)	31 ± 23 (69)	Mitotic exit and spindle checkpoint kinase
	gwl (2)	8%	2 ± 2 (112)	26 ± 10 (99)	Negative PP2A regulator and mitotic exit kinase
	ald	59%	52 (25)	88 (25)	Altered disjunction, chromosome separation kinase

235

236 **Table 1: Top hits from synthetic lethality screen**
237 Top hits from the synthetic lethality screen were grouped by gene function. Overall survival rate ratio was
238 determined by the following: (percentage of surviving larvae after RNAi and I-CreI induction) / (percentage
239 of surviving larvae after only RNAi induction). Those RNAi transgenes that resulted significant reduction in
240 survival (a ratio of less than 0.65) were considered for follow-up live analysis.
241

242 The acentrics are generated through I-CreI induced double-strand breaks. As expected,
243 RNAi knockdowns of DNA repair and cell cycle checkpoints exhibit synthetic lethality upon I-CreI
244 induction. Genes involved in DNA repair all exhibit strong synthetic lethality upon I-CreI induction.
245 DSB repair genes *spnA/Rad51* [34], *mus309* [35] and NHEJ gene *Ku80* [36] exhibited survival
246 ratios of 2%, 11%, and 29%, respectively (**Table 1**). The DNA damage checkpoint gene *tefu* (ATM
247 [37]) also results in a pronounced synthetic lethality (survival ratio of 43%). The screen also
248 yielded a number of microtubule-associated proteins. These included *msps* (microtubule
249 nucleation [38]), *asp* (astral microtubule organization [39]), *eb1* (plus-end microtubule binding
250 [40]), *klp68D* (kinesin motor protein [41]), and *map205* (microtubule stabilizer [42]). Given that
251 microtubule-based transport plays a key role in the poleward transport of the acentric
252 chromosome fragments [15], synthetic lethal interactions with microtubule-associated proteins
253 were expected. However, it was unclear whether microtubules and their associated proteins also
254 play a role in the initial separation of sister acentrics during the metaphase-to-anaphase transition.
255 The screen also yielded a large class of genes involved in chromatin organization. Synthetic lethal
256 interactions with chromatin organizing proteins were expected due to the presence of I-CreI
257 induced DSBs. This included *cap-D2* (condensin [43]), *chd1* (ATP-dependent chromatin
258 remodeler [44]), *sin3A* and *sir2* (histone deacetylases [45]), *chrac* (nucleosome mobilization [46]),
259 and *hp1* (heterochromatin protein [47]). Whether these are directly required for double-strand
260 break repair, separation and/or segregation of sister acentrics remains to be determined. In
261 accord with previous work, reduced levels of BubR1 kinase (spindle-assembly checkpoint protein)
262 also exhibited a pronounced synthetic lethality upon I-CreI induction [12]. The screen also yielded
263 two additional cell cycle kinases: *gwl* (greatwall kinase, an inhibitor of the cell cycle phosphatase
264 PP2A [48]) and *ald* (altered disjunction, chromosome segregation [49]). We chose to focus on
265 EB1 and Map205 due to their well-documented association with microtubules [40, 42]. Greatwall
266 was chosen for follow-up because previous studies demonstrated that this kinase is required for
267 sister separation of intact chromosomes [50].

268 **Live imaging analysis reveals the microtubule-associated proteins Map205 and EB1 and**
269 **Topo II are required for separation, but not segregation of sister acentrics.**

270 We conducted live imaging experiments on neuroblasts to investigate the effect of specific
271 RNAi-mediated gene knockdowns on acentric mitotic transmission. Each line contains an RFP-
272 tagged histone transgene facilitating live confocal analysis [51]. Based on previous studies
273 revealing the role of microtubules in acentric transmission [15], we initially focused on the
274 microtubule-stabilizing protein Map205 and the microtubule plus-end associated protein EB1.

275 In a wild-type background, the majority of acentrics line up at the outer edge of the
276 metaphase plate, separated from the main mass of intact chromosomes [12, 15]. As described
277 above and in previous publications, during anaphase sister acentrics remain paired on the
278 metaphase plate well after the separation of intact chromosomes (**Figure 4A**) [12, 15]. On
279 average, separation of sister acentrics occurs 148 seconds ± 44 (N=19) after separation of the
280 kinetochore-bearing chromosomes (**Table 2**). 83% (19/23) of acentric sister chromatid pairs
281 separate normally with sister acentrics going to opposite cell poles (**Figure 4C**). In the remaining
282 17% (4/23), acentric sister chromatids line up in metaphase, lag behind at the metaphase plate,
283 and segregate together to one pole of the cell (**Table 3**). Micronuclei form in telophase in 24%
284 (4/17) of neuroblasts expressing I-CreI micronuclei form in telophase (**Figure 4D**).

285 **Fig 4: EB1 RNAi knockdowns specifically disrupt acentric sister separation.** (A) Still frames of a time-
286 lapse movie of a mitotic neuroblast with I-CreI induced acentrics. Paired sister acentrics (white and yellow
287 arrowheads) lag behind at the spindle equator but eventually separate, segregate, and are reincorporated
288 into daughter nuclei. (B) Still frames of a time-lapse movie of a mitotic neuroblast with I-CreI induced
289 acentrics and expressing EB1 RNAi. Separation of paired sister acentrics (white and yellow arrowheads)
290 fails, resulting in sisters segregating to and incorporating into the same daughter nucleus. Bars, 2 μm. Time
291 in seconds. (Video 3) (C) Percentages of neuroblast divisions in which acentric sisters failed to completely
292 separate from one another. (D) Percentages of neuroblast divisions in which acentrics failed to incorporate
293 into daughter nuclei and formed one or more micronuclei.
294

295

296

	Avg ± SD (seconds)	N (acentric pairs)
Control	148 ± 44	19
MAP205 RNAi	97 ± 39 **	12
EB1 RNAi	142 ± 57	16
Topo II RNAi	226 ± 77 *	10
***gwl*^{1028}/*gwl*^{716}**	138 ± 49	22

Table 2: Sister separation of acentrics is delayed relative to sister separation of intact chromosomes
Average time (in seconds) for sister acentrics to initiate separation after sister kinetochore-bearing chromosomes separated. Time (average ± SD) measured from initiation of intact chromosome separation to initiation of acentric sister chromosome separation. Asterisks indicate statistical significance (**P=0.001, *P=0.003) as determined by two-sided Mann-Whitney tests.

	Fails to separate	Dissociate	Slides Apart	Unzip	N (acentric pairs)
Control	17%	13%	48%	22%	23
MAP205 RNAi	46%	9%	9%	36%	22
EB1 RNAi	47%	20%	13%	20%	30
Topo II RNAi	54%	14%	27%	5%	22
***gwl*^{1028}/*gwl*^{716}**	39%	11%	28%	22%	36

Table 3: Acentric separation occurs through three distinct modes
Acentric sister chromatids either fail to separate or separate from one another by three different modes: laterally sliding past one another, unzipping from one another, or simultaneously and evenly dissociating along their lengths.

Live imaging of acentric behavior in neuroblasts expressing Map205 RNAi revealed that 46% (10/22) of acentric sister chromatids do not separate from one another and segregate to one cell pole together, in comparison to 17% (4/23) in a wildtype background (**Figure 4C, Figure 5B, Table 3**). Additionally, after partial knockdown of Map205, sister acentrics separated from one another significantly earlier than acentrics in a wildtype background (P=0.001, Mann-Whitney test, **Table 2**). In spite of defects in acentric sister chromatid separation, their average poleward segregation velocity was normal (**Table 4**). Despite the increase in failed acentric separation, there was not an increase in micronuclei formation (21% compared to 24% in controls) (**Figure 4D**).

Fig 5: Knockdowns of EB1 and Map205 preferentially disrupt the sliding mode of acentric separation. (A) Model of different acentric orientations prior to separation. Polarity axis indicated by the dotted line. (B) Bar graph showing the percentage of acentric pairs that separate via simultaneous dissociation, sliding, or unzipping and the percentage of those that fail to separate. (C-G) Measurements of the frequency of each mode of acentric sister separation (x-axis) and the timing of acentric sister separation after the separation of intact chromosomes (y-axis). Each dot represents one acentric pair. Blue dots represent acentric pairs that were oriented perpendicular then parallel to the polarity axis prior to separation. Orange dots represent acentric pairs that were oriented parallel to the polarity axis prior to separation. Green dots represent acentric pairs that were oriented perpendicular to the polarity axis prior to separation. Boxes show interquartile ranges and lines show medians of the measured data. Asterisks indicate statistical significance (*P = 0.01, **P = 0.005, ***P = 0.009) when comparing the timing of acentric separation between separation modes. Statistical analysis was done using two-sided Mann-Whitney tests. Non-significant values had a P-value greater than 0.05.

	Avg velocity ± SD (nm/s)	N (individual acentrics)
Control	10 ± 4	26
MAP205 RNAi	12 ± 5	30
EB1 RNAi	10 ± 4	27
Topo II RNAi	12 ± 3	26
gwl^{1028}/gwl^{716}	8 ± 4 *	32

Table 4: Average velocities of acentric segregation
Depicted below are the velocities of individual acentrics as they segregate during anaphase. Velocity is measured in nanometers per second. Segregation velocity is defined as beginning when an acentric is clearly observed as separated from its sister and ends when the acentric reaches the daughter nucleus. Asterisks indicate statistical significance (*P=0.006) as determined by a two-sided Mann-Whitney test.

Live analysis of acentric behavior in neuroblasts expressing EB1 RNAi revealed that 47% (14/30) of acentric sister pairs fail to separate (**Figure 4C, Figure 5E, Table 3**). The failure of separation results in acentric sisters segregating together to a single cell pole (**Figure 4B, Movie S3**). Additionally, the delay in acentric separation and their rate of poleward segregation were normal (**Figure 5E, Table 2, Table 4**). There was also not an increase in micronuclei formation (15% compared to 24% in controls) (**Figure 4D**). This indicates that the Map205 and EB1 knockdowns are specifically disrupting sister separation of acentrics and have no effect on the latter stages of acentric transmission.

As described earlier, cohesin removal on the intact chromosomes and acentrics occurs simultaneously, yet acentric sisters remain paired. This raised the possibility of a role for DNA catenation in maintaining acentric pairing. Previous work demonstrated that DNA catenations

352 preserve sister chromatid cohesion in intact chromosomes until resolution by Topoisomerase II
353 (Topo II) at the metaphase-anaphase transition [52]. Topo II decatenates intertwined DNA
354 allowing sister chromatids to segregate to opposing poles of the cell. To test the role of DNA
355 catenation in maintaining acentric sister pairing, we knocked down levels of Topo II specifically in
356 the *Drosophila* neuroblast using the Gal4/UAS RNAi technique described above. Topo II
357 knockdowns revealed that 54% (12/22) of sister acentrics fail to separate and subsequently
358 segregate together to one pole (**Figure 6, Table 3, Movie S4**). Due to the lasting catenations
359 between acentric sisters, the initiation of acentric separation was further delayed in neuroblasts
360 expressing Topo II RNAi (Mann-Whitney test; P=0.003) (**Table 2**). Although acentric separation
361 is disrupted, their poleward segregation rate and their rate of micronuclei formation were normal
362 (**Figure 5F, Table 4, Figure 4D**).

363 **Fig 6: Acentrics appear to be held together by DNA catenations.** (A) Still images of a time- lapse
364 movie of a control neuroblast with I-CreI induced acentrics showing sister acentrics associated in early
365 anaphase (white arrows), lagging behind and ultimately separating and segregating to opposite poles (cyan
366 and magenta arrowheads). (B) Still images of a time-lapse movie of a neuroblast with partial knockdown of
367 Topoisomerase II using RNAi and I-CreI induced acentrics. Acentrics associate and lag behind in early
368 anaphase (white arrow), then fail to completely separate and segregate unequally (cyan and magenta
369 arrowheads). Bars, 2 μm. Time in seconds. (Movie S4) (C) Bar graph showing the quantification of acentric
370 behavior in control and Topo II RNAi neuroblasts with the failure of acentric sister separation in magenta
371 and the successful, even separation of acentric sisters in gray.
372

373 The screen also yielded the PP2A inhibitor Greatwall kinase (*gwl*) that controls the timing
374 and events of mitotic exit including sister chromatid separation [50]. Thus, we were particularly
375 interested in the dynamics of acentric separation and segregation when the levels of *gwl* were
376 reduced. This analysis uncovered that with reduced levels of *gwl*, 39% (14/36) of acentric sister
377 pairs failed to separate from one another (**Figure 4C, Figure 5B, Table 3**). Additionally, the delay
378 in acentric separation and the rate of micronuclei formation were normal (**Figure 5G, Table 2,**
379 **Figure 4D**). However, the average velocity of acentrics while segregating during anaphase was
380 significantly slower in *gwl* mutant background compared to acentrics in wildtype background
381 (P=0.006; Mann-Whitney test) (**Table 4**).
382

383 **EB1, Map205, Greatwall, and Topo II differentially influence the dynamics of**
384 **acentric separation.**

385 As described above, in a wild-type background acentrics exhibit three distinct patterns of
386 separation: sliding, unzipping, and simultaneous dissociation. Sliding is the most frequent
387 occurring 49% of the time, with unzipping and simultaneous dissociation occurring at frequencies
388 of 31% and 20%, respectively (**Figure 3E**). To determine the role of the genes identified above in
389 these distinct forms of acentric separation, we monitored the frequency of segregation patterns in
390 RNAi knockdowns of the candidate genes. Of those sister acentrics that successfully separated,
391 knockdowns of Map205, EB1, and Greatwall resulted in a decreased frequency of separation via
392 sliding (17%, 25%, 45%, respectively) compared to the control (58%) (**Figure 5**). Additionally,
393 Topoisomerase II resulted in a decreased the frequency of acentric separation via unzipping
394 (10%) compared to the control (26%) (**Figure 5**).

395 To determine if microtubule plus-ends preferentially accumulate around acentrics, I-CreI-
396 expressing neuroblasts were live imaged with EGFP-tagged EB1. Fluorescence intensities of both
397 GFP and RFP were measured and corrected for brightness in control neuroblasts (N=5) and I-
398 CreI-expressing neuroblasts (N=5). During mitosis, EB1 localizes along microtubules moving
399 towards the plus-ends (**Figure 7 and Movie S5**). Previous studies have shown that EB1 is
400 essential for generating antipolar forces on chromosomes [53, 54]. That finding together with our
401 finding that EB1 is required for sister acentric separation motivated us to examine EB1 localization
402 on the acentrics (**Figure 7**). We find the concentration of EB1 is not significantly increased on or
403 near the acentrics ($P > 0.05$, two sample t-test; **Figure 7**). Thus, while EB1 and the acentrics co-
404 localize, the pattern of EB1 comets is not altered in the presence of acentrics. While these data
405 are consistent with a role for EB1 in acentric sister separation, there is not an increase in
406 recruitment and accumulation of EB1 at the acentric.

407 **Fig 7: Acentrics travel poleward in late anaphase while associated with EB1.** EB1 is in green and
408 chromosomes are in magenta. (A) Still images from a time-lapse movie of a control neuroblast from
409 metaphase (0 s) through telophase (85 s). (B) Still images from a time-lapse movie of a mitotic neuroblast

410 with I-CreI induced acentrics from metaphase (0 s) through telophase (135 s) (Movie S5). The intact
411 chromosomes and acentrics initiate sister separation at the 15 s and 40 s timepoints, respectively. Sister
412 acentrics (white arrowheads) separate and move toward opposite cell poles while associated with EB1. (C)
413 Line graph from a compilation of five control videos showing the corrected fluorescence intensities in
414 arbitrary units (AU) of EB1 (green) and chromosomes (magenta). Corrected fluorescence intensities were
415 calculated within the yellow boxes at the time points 15, 20, 25, 30, 35 seconds after anaphase onset. (D)
416 Line graph from a compilation of five videos of I-CreI-expressing neuroblasts showing the corrected
417 fluorescence intensities in arbitrary units (AU) of EB1 (green) and chromosomes (magenta). Corrected
418 fluorescence intensities were calculated within the yellow boxes at the time points 15, 25, 30, 40, 50
419 seconds after anaphase. Bars, 2 μm. Time in seconds. Error bars represent SDs of the fluorescent
420 intensities at all points tested.
421

422 **DISCUSSION**

423 These studies are based on the unexpected finding that sister chromosome fragments
424 lacking a kinetochore undergo relatively normal separation. We sought to identify the kinetochore
425 independent forces driving acentric sister chromatid separation. A key finding is that while cohesin
426 removal occurs simultaneously on intact and acentric chromosomes, sister separation of the latter
427 is significantly delayed. An explanation for this delay comes from studies of intact chromosomes
428 demonstrating that once cohesin is removed, sister acentrics remain held together through DNA
429 catenations [52, 55, 56]. Catenations are concentrated at the centromeric DNA and opposing
430 kinetochore microtubule interactions likely provide the resolving force [57-61]. Support for this
431 conclusion comes from studies of chromosome rearrangements in which centromeric
432 heterochromatin is displaced from the centromere [31]. Sister chromatin separation is specifically
433 delayed in these regions resulting in localized stretching during anaphase. A likely consequence
434 of being displaced from the centromere is that the ectopic heterochromatic regions no longer
435 experience sufficient kinetochore forces required to efficiently resolve sister DNA catenations. In
436 light of these studies, it is likely that acentric sisters remain associated well after separation of the
437 intact chromosomes through DNA catenations. This conclusion is supported by our finding that
438 reductions in the Topoisomerase II levels specifically disrupt acentric sister separation. As
439 described below, our studies suggest both plus-end and lateral microtubule interactions with the
440 acentrics provide the alternative force driving sister separation.

441 Intact chromosomes align perpendicular to the spindle. In contrast, we find acentric
442 chromosomes align either perpendicular or parallel to the spindle. When aligned parallel to the
443 spindle, acentrics travel with one tip leading towards the cell pole, possibly due to microtubule
444 lateral interactions with acentrics. Without a kinetochore, a combination of lateral and plus-end
445 microtubule interactions likely determines the final orientation of acentrics on the metaphase
446 plate. In addition to the multiple orientations, acentrics undergo distinct patterns of sister
447 separation that we have termed sliding, unzipping and simultaneous dissociation. Sliding of
448 sisters past one another toward opposite poles is the most common mode of acentric separation.
449 This mode occurs primarily when sister acentrics are oriented parallel to the spindle just prior to
450 separation suggesting lateral microtubule interactions provide the force driving this mode of
451 acentric separation (**Figure 3A, Figure 5C**). While sister separation of all acentrics is delayed
452 relative to intact chromosomes, the delay is much more pronounced for acentrics that undergo
453 separation by sliding. The delay may in part be due to the additional time it takes to establish the
454 multiple lateral interactions required to generate sufficient separation force. It is likely
455 chromokinesins provide the force driving separation, but these have yet to be identified.

456 In contrast to sliding, sister separation by unzipping occurs primarily when the acentrics
457 are oriented perpendicular to the spindle just prior to separation suggesting a limited role for lateral
458 microtubule interactions (**Figure 3B, Figure 5C**). During unzipping, acentrics generally initiate
459 separation at their broken ends with completion of separation occurring at the telomeres. The
460 delay of acentric separation by unzipping is much less than the delay observed for separation
461 by sliding. Previous studies demonstrated that the acentric and its centric partner are connected
462 via a DNA tether [12]. The preference for initiation of separation at the broken-ends suggests that
463 a DNA tether connecting the broken end to the kinetochore-bearing fragment may provide the
464 initial separation force (**Figure 3B**). While this tether is not thought to provide the force driving
465 acentric segregation [15], because of its association with the broken end of the acentric, it may
466 drive the initial stage of unzipping. In contrast to separation by sliding, telomeres are always

467 aligned in sisters that separate by unzipping (**Figure 3E, Figure 3F**). This suggests maintaining
468 gene-for- gene sister pairing is essential for this form of separation.

469 The third mode of acentric separation, simultaneous dissociation, is characterized by a
470 synchronized separation along the entire length of sister acentrics (**Figure 3C**). While sister
471 separation via simultaneous dissociation favors the perpendicular orientation, this bias is much
472 less dramatic compared to the unzipping mode (**Figure 5C**). The most distinguishing feature of
473 this form of separation is the high frequency in which sister acentrics aligned with their telomeres
474 opposed (33% compared to 14% and 0% for sliding and unzipping separation, respectively)
475 (**Figure 3F**). This high frequency of unaligned telomeres suggests weak connections between
476 sisters and that sister pairing is not required.

477 Synthetic lethal screens have proven an effective means of identifying factors required for
478 the successful mitotic transmission of acentric chromosome fragments [12, 15]. These screens
479 have identified proteins required for poleward transmission and final incorporation of acentrics
480 into the telophase nucleus. Here we focused on identifying genes required for successful
481 separation of sister acentrics. Of the 117 candidate genes screened, we identified 23 RNAi
482 knockdowns/mutations that resulted in a significant lethality upon acentric induction (**Table 1**).
483 Live analysis secondary screening revealed knockdowns of EB1 and Map205, and the cell cycle
484 kinase Greatwall resulted in dramatic defects in acentric sister separation. Live imaging also
485 revealed reducing levels of Topoisomerase II severely disrupted sister acentric separation.

486 Given that previous studies demonstrated the chromokinesin Klp3A is required for acentric
487 poleward transport [15], it is not surprising that microtubule-associated proteins also play a key
488 role in separation of acentric sisters. Reduced levels of EB1 and Map205 greatly increase the
489 frequency of failed sister separation. EB1 is a plus-end tracking protein that associates with a
490 number of regulatory proteins and is essential for generating anti-polar forces on the
491 chromosomes [62]. EB1 knockdowns most dramatically reduce the frequency of acentric
492 separation via sliding. In addition, for those acentric sisters that did separate by sliding in EB1

493 knockdowns, separation was greatly delayed. As lateral interactions between the microtubules
494 and chromatin are likely to drive sister separation by sliding, we suspect plus-end directed EB1
495 forces may play a role in orienting the acentric in order to establish lateral interactions. Support
496 for this idea comes from the finding of a synthetic lethal interaction between I-CreI induction and
497 reductions in the levels of Nod, a non-motile chromokinesin that associates with EB1 and is
498 involved in chromosome segregation [15, 63-65]. Surprisingly, a previous study in our lab found
499 no effect on acentric segregation in mutations in Nod [15]. Examining movies from this analysis
500 revealed no significant difference in acentric sister separation in a loss-of-function *nod* mutant
501 compared to the control (**Table S2**). Map205 is a microtubule-associated protein required for
502 targeting Polo kinase to spindle microtubules [42]. Thus, it is likely that the effect of the Map205
503 knockdowns on acentric sister separation is through disruption of Polo localization. Previous
504 studies demonstrated that Polo localizes to the DNA tether associated with the acentric and Polo
505 knockdowns disrupted acentric transmission with sister acentrics remaining on the metaphase
506 plate [12]. As with EB1, reductions in Map205 levels dramatically reduce the frequency of acentric
507 separation by sliding suggesting a disruption in lateral interactions between the acentrics and the
508 microtubules. While much evidence indicates that Polo functions at the centromere during sister
509 separation, our studies of the effects of Map205 and Polo knockdowns suggest that it is also
510 involved in promoting chromatid/spindle interactions that are independent of the centromere.
511 Reducing the levels of Topoisomerase II leads to a significant increase in failed separation of
512 sister acentrics, supporting the conclusion that once cohesin is removed sister acentrics remain
513 held together through DNA catenation. We suspect that reduced Topoisomerase II levels disrupt
514 sister separation of the acentrics more profoundly than that of intact chromosomes because the
515 latter primarily rely on kinetochore forces to resolve DNA catenations. Of the four mutants
516 analyzed through live analysis, reductions in Topoisomerase levels had the greatest effect of the
517 unzipping mode of acentric sister separation. This result is interesting given our finding that the

518 unzipping mode of acentric separation is likely the most reliant on sister pairing and consequently
519 are likely to be highly catenated.

520 Taken together, these data support a model in which multiple forces drive the separation
521 of sister acentrics. Acentrics that separate by sliding and unzipping tend to be oriented parallel
522 and perpendicular to the spindle, respectively. Unzipping could be initially driven by the DNA
523 tether, which connects the acentric to its centric partner, to initially separate one end of the
524 acentrics. Then, a combination of Topoisomerase II activity and microtubule forces could facilitate
525 the separation of the other end of the acentrics. Because the partial knockdown of Topoisomerase
526 II leads to a decreased frequency of acentrics unzipping, we hypothesize that the resolution of
527 DNA catenations by Topoisomerase II underlies the unzipping mode of separation. Due to the
528 finding that the tether does not appear to provide segregation forces on the acentrics [15], sliding
529 is likely driven by lateral microtubule interactions and possibly motor proteins. This is further
530 supported by the orientation of acentrics parallel to the axis of polarity and the association of EB1
531 and bundling of microtubules around acentrics in early anaphase. It remains unclear if acentrics
532 are directly interacting with microtubules or if microtubule-associated proteins are mediating the
533 interaction with acentrics. There is not an obvious mechanism for the simultaneous dissociation
534 of sister acentrics and is likely driven by a combination of factors (**Figure 8**). EB1 and Map205
535 may be required to establish microtubule interactions with the acentric, while in the absence of a
536 kinetochore high levels of Topoisomerase are needed to resolve DNA catenations between
537 sisters.

538 **Fig 8: Schematic showing distinct modes of acentric separation.** At some point during the metaphase-
539 to-anaphase transition, acentrics that separate by sliding orient parallel to the spindle and slide past one
540 another. This is likely driven by lateral associations between the microtubules and acentrics. The unzipping
541 mode occurs when separation initiates at the broken end followed by separation of sister telomeres. It may
542 be that the initial separation is driven by the DNA tether connecting the centric and acentric fragments.
543 Separation across the entire length of the acentric is referred to as simultaneous dissociation. It may be
544 that the DNA tether and acentric-microtubule interactions contribute equally for sister acentrics that
545 separate by simultaneous dissociation. (Chromosomes in magenta, microtubules in green, cohesin in cyan,
546 telomeres in orange).
547

It should be noted that although these mutants resulted in a high frequency of failed acentric sister separation, we did not observe an equivalent increase in micronuclei. In contrast, mutants that disrupted acentric poleward transport or the final stages of incorporation into daughter nuclei resulted in an accompanying increase in micronuclei [66-68]. This indicates that the knockdowns in the genes identified in this study specifically disrupt acentric sister separation as the subsequent transmission occurs normally to allow incorporation of the acentric into the daughter nuclei. This interpretation is in accord with a model that acentrics experience different forces at different stages of their separation, transmission, and incorporation into daughter nuclei [68].

There are numerous examples of lateral interactions between spindle microtubules and intact chromosomes indicating that non-kinetochore forces influence anaphase chromosome kinetics [69-71]. However, it has been difficult to pursue the underlying mechanisms because of the dominance of kinetochore forces during anaphase. In analogy with studies of spindle formation in cells lacking centrosomes that led to the discovery of unsuspected, yet conserved, chromosome-based mechanisms of spindle assembly, examining the mitotic behavior of acentric chromosomes without a kinetochore will provide insights into the kinetochore independent forces acting on intact chromosomes [70, 71].

581 **MATERIALS AND METHODS**

582 Fly Stocks

583 All stocks were raised on standard *Drosophila* media at room temperature (20-22°C) as
584 previously described [72]. For generating acentrics, a transgenic fly line bearing the I-CreI
585 endonuclease under heat-shock 70 promoter were kindly provided by Kent Golic at The
586 University of Utah. For synthetic lethality screen, the ubiquitous Gal4 driver under the control of
587 an actin enhancer (Act5) was used (#25708 from Bloomington). Dominant negative allele of
588 ISWI was kindly provided by John Tamkun at UC Santa Cruz. Greatwall hypomorphs (*gwl*^{1080,}
589 $^{716, 180, and 2790}$) were kindly provided by Michael Goldberg at Cornell University. The line with
590 *rad21-EGFP* transgene were kindly provided by Stefan Heidmann at University of Bayreuth.

591

592 Synthetic Lethality Screen

593 Third instar progeny with genotype Act5-Gal4/+; I-CreI, Sb/UAS-RNAi were collected from
594 parental genotypes Act5-Gal4/CyO-GFP; I-CreI, Sb/TM6B and were heat shocked for 1.5 hours
595 at 37°C (unless otherwise indicated). After heat shock, the vials were set-aside at room
596 temperature for 10-15 days until adult flies emerged. Synthetic lethality was calculated as the %
597 of larvae that develop into adulthood [12, 15]. Control progeny with genotype Act5-Gal4/+;
598 Sb/UAS-RNAi from parents with the genotype Act5-Gal4/CyO-GFP; Sb/TM6B and UAS-RNAi
599 were heat-shocked for 1.5 hours at 37°C.

600

601 Live analysis of acentric behavior in *Drosophila* third instar neuroblasts

602 As previously described, acentric chromosome fragments were induced by I-CreI expression
603 (under heat shock 70 promoter) in 3rd instar larvae by a 1-hour 37°C heat shock followed by a 1-
604 hour recovery period at room temperature [12]. The larval brains from third instar larvae were
605 dissected in PBS and then transferred to a slide with 20 µl of PBS. A coverslip was dropped on
606 PBS with brain and the excess PBS was wicked out from edge of coverslip to induce squashing

607 of brain between slide and coverslip. For live analysis, the edge of coverslip was sealed with
608 halocarbon and was imaged as described below. Neuroblast divisions in all images were from
609 female 3rd instar larvae.
610
611 Microscopy and image acquisition
612 *Wide-field microscopy*
613 Time-lapse imaging for Figure 4C, 4D, 5C, and 6 were performed using a Leica DM16000B
614 wide-field inverted microscope equipped with a Hamamatsu electron-multiplying charge coupled
615 device camera (ORCA 9100-02) with a binning of 1 and a 100x Plan-Apochromat objective with
616 NA 1.4. Successive time points were filmed at 20 s. RFP (585 nm) and GFP (508 nm)
617 fluorophores were imaged. Samples were imaged in PBS and at room temperature (20-22°C).
618 Widefield images were acquired with Leica Application Suite Advanced Fluorescence Software
619 and 3D deconvolved using AutoQuant X2.2.0 software.
620
621 *Spinning-disk microscopy*
622 Images in Figures 1, 2, 3, 4, 6, and 7 were acquired with an inverted Nikon Eclipse TE2000-E
623 spinning disk (CSLI-X1) confocal microscope equipped with a Hamamatsu electron-multiplying
624 charge coupled device camera (ImageEM X2) with a 100X 1.4 NA oil-immersion objective.
625 Samples were imaged in PBS and at room temperature (20-22°C). Images were acquired with
626 MicroManager 1.4 software. Time-lapse fluorescent images of neuroblasts divisions were done
627 with 120 and 100 ms exposures for GFP and RFP respectively with 0.5 μm Z-steps. Time-lapse
628 videos with both GFP and RFP were done every 5 to 9 seconds and time-lapse movies with
629 RFP alone were done every 5 seconds. Figures were assembled in Adobe Illustrator. Selected
630 stills (both experimental and control) were processed with ImageJ (http://rsb.info.nih.gov/ij/).
631
632
633

634 Measurements
635
636 In Figure 2C, relative fluorescence intensities of chromosomes (H2Av-RFP) and cohesin
637 (Rad21-EGFP) were done using the plot profile function in ImageJ of the region outlined around
638 acentrics and the main mass of chromosomes. In Figures 7C and 7D, relative fluorescence
639 intensities of acentrics (H2Av-RFP) and EB1 (EB1-EGFP) were done using the plot profile
640 function in ImageJ of the region outlined around acentrics in I-CreI expressing neuroblasts and
641 the region outlined around the spindle midzone in control neuroblasts. For statistical analyses,
642 unpaired two-sided t-tests and two-sided Mann-Whitney-Wilcoxon tests were used. Unpaired
643 two-sided t-tests were performed in Prism Version 8 (GraphPad Software). Two-sided Mann-
644 Whitney-Wilcoxon tests were performed in R (R Core Team) and Prism Version 8 (GraphPad
645 Software).
646
647 **ACKNOWLEDGEMENTS**
648
649 We would like to thank Dr. Susan Strome, Dr. William Saxton, and Dr. John Tamkun for use of
650 their equipment and providing reagents. We thank Dr. Benjamin Abrams for his advice and
651 technical expertise regarding microscopy experiments. We thank Dr. Kent Golic for providing us
652 with the transgenic fly line bearing the I-CreI endonuclease. We thank Dr. Michael Goldberg for
653 providing us with Greatwall hypomorph flies. We thank Dr. Stefan Heidmann for providing us
654 with the transgenic fly line bearing *rad21-EGFP*. We thank H. Vicars' service dog Teddy Bear
655 for his guidance and support.
656
657 Funding for these studies was provided by National Institutes of Health grant
658 NIH1RO1GM120321 awarded to W. Sullivan.
659
660 The authors declare no competing financial interests.
661
662

REFERENCES

1. Ermolaeva MA, Schumacher B. Systemic DNA damage responses: Organismal adaptations to genome instability. Trends Genet. 2014;30(3):95–102. pmid:24439457; PubMed Central PMCID: PMC4248340

2. Mikhailov A, Cole RW, Rieder CL. DNA Damage during Mitosis in Human Cells Delays the Metaphase/Anaphase Transition via the Spindle-Assembly Checkpoint. Current Biology. 2002;12(21):1797–806. pmid:12419179

3. Royou A, Macias H, Sullivan W. The Drosophila Grp/Chk1 DNA Damage Checkpoint Controls Entry into Anaphase. Current Biology. 2005;15(4):334–9. pmid:15723794

4. Coutelier H, Xu Z. Adaptation in replicative senescence: a risky business. Curr Genet. 2019;65(3):711–6. pmid:30637477

5. Kanda T, Wahl GM. The dynamics of acentric chromosomes in cancer cells revealed by GFP-based chromosome labeling strategies. J Cell Biochem Suppl. 2000; Suppl 35:107–14. pmid:11389539

6. LaFountain JR, Oldenbourg R, Cole RW, Rieder CL. Microtubule Flux Mediates Poleward Motion of Acentric Chromosome Fragments during Meiosis in Insect Spermatocytes. Mol Biol Cell. 2001;12(12):4054–65. pmid:11739800; PubMed Central PMCID: PMC60775

7. Fenech M, Kirsch-Volders M, Natarajan AT, Surralles J, Crott JW, Parry J, et al. Molecular mechanisms of micronucleus, nucleoplasmic bridge and nuclear bud formation in mammalian and human cells. Mutagenesis. 2011;26(1):125–32. pmid:21164193

8. Bajer A. Cine-micrographic studies on chromosome movements in β-irradiated cell. Chromosoma. 1958;9:319-331. pmid:13608834

9. Liang H, Wright WH, Cheng S, He W, Berns MW. Micromanipulation of chromosomes in PTK2 cells using laser microsurgery (optical scalpel) in combination with laser-induced optical force (optical tweezers). Experimental cell research. 1993;204(1):110–20. pmid:8416789

10. Khodjakov A, Cole RW, Bajer AS, Rieder CL. The force for poleward chromosome motion in Haemanthus cells acts along the length of the chromosome during metaphase but only at the kinetochore during anaphase. J Cell Biol. 1996;132(6):1093–104. pmid:8601587; PubMed Central PMCID: PMC2120764

11. Kanda T, Sullivan KF, Wahl GM. Histone–GFP fusion protein enables sensitive analysis of chromosome dynamics in living mammalian cells. Current Biology. 1998;8(7):377–85. pmid:9545195

12. Royou A, Gagou ME, Karess R, Sullivan W. BubR1- and Polo-Coated DNA Tethers Facilitate Poleward Segregation of Acentric Chromatids. Cell. 2010;140(2):235–45. pmid:20141837; PubMed Central PMCID: PMC2969851

13. Bretscher HS, Fox DT. Proliferation of Double Strand Break Resistant Polyploid Cells Requires Drosophila FANCD2. Dev Cell. 2016;37(5):444–57. pmid:27270041; PubMed Central PMCID: PMC4901310

14. Platero JS, Ahmad K, Henikoff S. A Distal Heterochromatic Block Displays Centromeric Activity When Detached from a Natural Centromere. Molecular Cell. 1999;4(6):995–1004. pmid:10635324

15. Karg T, Elting MW, Vicars H, Dumont S, Sullivan W. The chromokinesin Klp3a and microtubules facilitate acentric chromosome segregation. J Cell Biol. 2017;216(6):1597–608. pmid:28500183; PubMed Central PMCID: PMC5461011
16. Kanda T, Otter M, Wahl GM. Mitotic segregation of viral and cellular acentric extrachromosomal molecules by chromosome tethering. J Cell Sci. 2001; 114:49-58. pmid:11112689

17. Ishii K, Ogiyama Y, Chikashige Y, Soejima S, Masuda F, Kakuma T, et al. Heterochromatin Integrity Affects Chromosome Reorganization After Centromere Dysfunction. Science. 2008;321(5892):1088–91. pmid:18719285

18. Ohno Y, Ogiyama Y, Kubota Y, Kubo T, Ishii K. Acentric chromosome ends are prone to fusion with functional chromosome ends through a homology-directed rearrangement. Nucleic Acids Res. 2016;44(1):232–44. pmid:26433224; PubMed Central PMCID: PMC4705696

19. Rong YS, Titen SW, Xie HB, Golic MM, Bastiani M, Bandyopadhyay P, et al. Targeted mutagenesis by homologous recombination in D. melanogaster. Genes Dev. 2002;16(12):1568–81. pmid:12080094; PubMed Central PMCID: PMC186348

20. Maggert KA, Golic KG. Highly Efficient Sex Chromosome Interchanges Produced By I-CreI Expression in Drosophila. Genetics. 2005;171(3):1103–14. pmid:16020774; PubMed Central PMCID: PMC1456814

21. Paredes S, Maggert KA. Ribosomal DNA contributes to global chromatin regulation. Proc Natl Acad Sci U S A. 2009;106(42):17829–34. pmid:19822756; PubMed Central PMCID: PMC2764911

22. Golic MM, Golic KG. A simple and rapid method for constructing ring-X chromosomes in Drosophila melanogaster. Chromosoma. 2011;120(2):159–64. pmid:21085980; PubMed Central PMCID: PMC4454366

23. Warecki B, Sullivan W. Mechanisms driving acentric chromosome transmission. Chromosome Res. 2020;Online ahead of print. pmid:32712740

24. Guacci V, Koshland D, Strunnikov A. A Direct Link between Sister Chromatid Cohesion and Chromosome Condensation Revealed through the Analysis of MCD1 in S. cerevisiae. Cell. 1997;91(1):47–57. pmid:9335334; PubMed Central PMCID: PMC2670185

25. Michaelis C, Ciosk R, Nasmyth K. Cohesins: Chromosomal Proteins that Prevent Premature Separation of Sister Chromatids. Cell. 1997;91(1):35–45. pmid:9335333

26. Uhlmann F, Lottspeich F, Nasmyth K. Sister-chromatid separation at anaphase onset is promoted by cleavage of the cohesin subunit Scc1. Nature. 1999;400(6739):37–42. pmid:10403247

27. Uhlmann F, Wernic D, Poupart M-A, Koonin EV, Nasmyth K. Cleavage of Cohesin by the CD Clan Protease Separin Triggers Anaphase in Yeast. Cell. 2000;103(3):375–86. pmid:11081625

28. Oliveira RA, Hamilton RS, Pauli A, Davis I, Nasmyth K. Cohesin cleavage and Cdk inhibition trigger formation of daughter nuclei. Nat Cell Biol. 2010;12(2):185–92. pmid:20081838; PubMed Central PMCID: PMC3284228

29. Gutiérrez-Caballero C, Cebollero LR, Pendás AM. Shugoshins: from protectors of cohesion to versatile adaptors at the centromere. Trends in Genetics. 2012;28(7):351–60. pmid:22542109

30. Asbury CL. Anaphase A: Disassembling Microtubules Move Chromosomes toward Spindle Poles. Biology. 2017;6(1):15. pmid:28218660; PubMed Central PMCID: PMC5372008

31. Oliveira RA, Kotadia S, Tavares A, Mirkovic M, Bowlin K, Eichinger CS, et al. Centromere-Independent Accumulation of Cohesin at Ectopic Heterochromatin Sites Induces Chromosome Stretching during Anaphase. PLoS Biol. 2014;12(10):e1001962. pmid:25290697; PubMed Central PMCID: PMC4188515

32. Urban E, Nagarkar-Jaiswal S, Lehner CF, Heidmann SK. The Cohesin Subunit Rad21 Is Required for Synaptonemal Complex Maintenance, but Not Sister Chromatid Cohesion, during Drosophila Female Meiosis. PLoS Genet. 2014;10(8):e1004540. pmid:25101996; PubMed Central PMCID: PMC4125089

33. Cenci G, Siriaco G, Raffa GD, Kellum R, Gatti M. The Drosophila HOAP protein is required for telomere capping. Nat Cell Biol. 2003;5(1):82–4. pmid:12510197

34. Staeva-Vieira E, Yoo S, Lehmann R. An essential role of DmRad51/SpnA in DNA repair and meiotic checkpoint control. EMBO J. 2003;22(21):5863–74. pmid:14592983; PubMed Central PMCID: PMC275421

35. McVey M, Andersen SL, Broze Y, Sekelsky J. Multiple Functions of Drosophila BLM Helicase in Maintenance of Genome Stability. Genetics. 2007;176(4):1979–92. pmid:17507683; PubMed Central PMCID: PMC1950607

36. Melnikova L, Biessmann H, Georgiev P. The Ku Protein Complex Is Involved in Length Regulation of Drosophila Telomeres. Genetics. 2005;170(1):221–35. pmid:15781709; PubMed Central PMCID: PMC1449706

37. Oikemus SR, McGinnis N, Queiroz-Machado J, Tukachinsky H, Takada S, Sunkel CE, et al. Drosophila atm/telomere fusion is required for telomeric localization of HP1 and telomere position effect. Genes Dev. 2004;18(15):1850–61. pmid:15256487; PubMed Central PMCID: PMC517405

38. Moon W, Hazelrigg T. The Drosophila Microtubule-Associated Protein Mini Spindles Is Required for Cytoplasmic Microtubules in Oogenesis. Current Biology. 2004;14(21):1957–61. pmid:15530399

39. Saunders RDC, Avides M do C, Howard T, Gonzalez C, Glover DM. The Drosophila Gene abnormal spindle Encodes a Novel Microtubule-associated Protein That Associates with the Polar Regions of the Mitotic Spindle. J Cell Biol. 1997;137(4):881–90. pmid:9151690; PubMed Central PMCID: PMC2139842

40. Rogers SL, Rogers GC, Sharp DJ, Vale RD. Drosophila EB1 is important for proper assembly, dynamics, and positioning of the mitotic spindle. J Cell Biol. 2002;158(5):873–84. pmid:12213835; PubMed Central PMCID: PMC2173155

41. Pesavento PA, Stewart RJ, Goldstein LS. Characterization of the KLP68D kinesin-like protein in Drosophila: possible roles in axonal transport. The Journal of Cell Biology. 1994;127(4):1041–8. pmid:7525600; pmid:7525600; PubMed Central PMCID: PMC2200055

42. Archambault V, D'Avino PP, Deery MJ, Lilley KS, Glover DM. Sequestration of Polo kinase to microtubules by phosphopriming-independent binding to Map205 is relieved by phosphorylation at a CDK site in mitosis. Genes Dev. 2008;22(19):2707–20. pmid:18832073; PubMed Central PMCID: PMC2559908

43. Savvidou E, Cobbe N, Steffensen S, Cotterill S, Heck MMS. Drosophila CAP-D2 is required for condensin complex stability and resolution of sister chromatids. Journal of Cell Science. 2005;118(11):2529–43. pmid:15923665

44. Stokes DG, Tartof KD, Perry RP. CHD1 is concentrated in interbands and puffed regions of Drosophila polytene chromosomes. Proc Natl Acad Sci USA. 1996;93(14):7137–42. pmid:8692958; PubMed Central PMCID: PMC38949

45. Feller C, Forné I, Imhof A, Becker PB. Global and Specific Responses of the Histone Acetylome to Systematic Perturbation. Molecular Cell. 2015;57(3):559–71. pmid:25578876

46. Corona DFV, Eberharter A, Budde A, Deuring R, Ferrari S, Varga-Weisz P, et al. Two histone fold proteins, CHRAC-14 and CHRAC-16, are developmentally regulated subunits of chromatin accessibility complex (CHRAC). EMBO J. 2000;19(12):3049–59. pmid:10856248; PubMed Central PMCID: PMC203371

47. Eissenberg JC, Elgin SCR. HP1a: A Structural Chromosomal Protein Regulating Transcription. Trends Genet. 2014;30(3):103–10. pmid:24555990; PubMed Central PMCID: PMC3991861

48. Yu J, Fleming SL, Williams B, Williams EV, Li Z, Somma P, et al. Greatwall kinase: a nuclear protein required for proper chromosome condensation and mitotic progression in Drosophila. J Cell Biol. 2004;164:487-492. pmid:14970188; PubMed Central PMCID: PMC2171981

49. O'Tousa J. Meiotic chromosome behavior influenced by mutation-altered disjunction in Drosophila melanogaster females. Genetics. 1982;102:503-524. pmid:6816677; PubMed Central PMCID: PMC1201954

50. Voets E, Wolthuis RMF. MASTL is the human orthologue of Greatwall kinase that facilitates mitotic entry, anaphase and cytokinesis. Cell Cycle. 2010;9(17):3591-601. pmid:20818157

51. Schuh M, Lehner CF, Heidmann S. Incorporation of Drosophila CID/CENP-A and CENP-C into centromeres during early embryonic anaphase. Curr Biol. 2007;17(3):237-243. pmid:17222555

52. Porter ACG, Farr CJ. Topoisomerase II: untangling its contribution at the centromere. Chromosome Res. 2004;12(6):569–83. pmid:15289664

53. Tirnauer JS, Bierer BE. EB1 proteins regulate microtubule dynamics, cell polarity, and chromosome stability. J Cell Biol. 2000;149(4):761-6. pmid:10811817; PubMed Central PMCID: PMC2174556

54. Vitre B, Coquelle FM, Heichette C, Garnier C, Chrétien D, Arnal I. EB1 regulates microtubule dynamics and tubulin sheet closure in vitro. Nat Cell Biol. 2008;10(4):415-21. pmid:18364701

55. Toyoda Y, Yanagida M. Coordinated Requirements of Human Topo II and Cohesin for Metaphase Centromere Alignment under Mad2-dependent Spindle Checkpoint Surveillance. Mol Biol Cell. 2006;17(5):2287–302. pmid:16510521; PubMed Central PMCID: PMC1446084

56. Murray AW, Szostak JW. Chromosome Segregation in Mitosis and Meiosis. Annual Review of Cell Biology. 1985;1(1):289–315. pmid:3916318

57. Farcas A-M, Uluocak P, Helmhart W, Nasmyth K. Cohesin's Concatenation of Sister DNAs Maintains Their Intertwining. Mol Cell. 2011;44(1–3):97–107. pmid:21981921; PubMed Central PMCID: PMC3240746

58. Wang LH-C, Mayer B, Stemmann O, Nigg EA. Centromere DNA decatenation depends on cohesin removal and is required for mammalian cell division. Journal of Cell Science. 2010;123(5):806–13. pmid:20144989

59. Kenney RD, Heald R. Essential roles for cohesin in kinetochore and spindle function in Xenopus egg extracts. Journal of Cell Science. 2006;119(24):5057–66. pmid:17158911

60. Baxter J, Sen N, Martinez VL, De Carandini MEM, Schvartzman JB, Diffley JFX, et al. Positive Supercoiling of Mitotic DNA Drives Decatenation by Topoisomerase II in Eukaryotes. Science. 2011;331(6022):1328–32. pmid:21393545

61. Piskadlo E, Oliveira RA. A Topology-Centric View on Mitotic Chromosome Architecture. Int J Mol Sci. 2017;18(12):2751. pmid:29258269; PubMed Central PMCID: PMC5751350

62. Nehlig A, Molina A, Rodrigues-Ferreira S, Honoré S, Nahmias C. Regulation of end-binding protein EB1 in the control of microtubule dynamics. Cell Mol Life Sci. 2017;74(13):2381–93. pmid:28204846

63. Theurkauf WE, Hawley RS. Meiotic spindle assembly in Drosophila females: Behavior of nonexchange chromosomes and the effects of mutations in the nod kinesin-like protein. J Cell Biol. 1992;116:1167-1180. pmid:1740471; PubMed Central PMCID:PMC2289365

64. Ye AA, Verma V, Maresca TJ. NOD is a plus end–directed motor that binds EB1 via a new microtubule tip localization sequence. J Cell Biol. 2018;217(9):3007–17. pmid:29899040; PubMed Central PMCID: PMC6122986

65. Afshar K, Barton NR, Hawley RS, Goldstein LSB. DNA binding and meiotic chromosomal localization of the Drosophila nod kinesin-like protein. Cell. 1995;81:129-138. pmid:7720068

66. Karg T, Warecki B, Sullivan W. Aurora B–mediated localized delays in nuclear envelope formation facilitate inclusion of late-segregating chromosome fragments. Mol Biol Cell. 2015;26(12):2227–41. pmid:25877868; PubMed Central PMCID: PMC4462941

67. Warecki B, Sullivan W. Micronuclei formation is prevented by Aurora B-mediated exclusion of HP1a from late-segregating chromatin in Drosophila. Genetics. 2018;210(1):171-187. pmid:29986897; PubMed Central PMCID: PMC6116970

68. Warecki B, Ling X, Bast I, Sullivan W. ESCRT-III–mediated membrane fusion drives chromosome fragments through nuclear envelope channels. Journal of Cell Biology. 2020;219(3):e201905091. pmid:32032426; PubMed Central PMCID: PMC7054997

69. Laband K, Le Borgne R, Edwards F, Stefanutti M, Canman JC, Verbavatz JM, et al. Chromosome segregation occurs by microtubule pushing in oocytes. Nature Comm. 2017;8(1):1499. pmid:29133801; PubMed Central PMCID: PMC5684144

70. Heald R, Tournebize R, Blank T, Sandaltzopoulos R, Becker P, Hyman A, et al. Self-organization of microtubules into bipolar spindles around artificial chromosomes in Xenopus egg extracts. Nature. 1996;382(6590):420-5. pmid:8684481

71. Fuge H. Non-kinetochore transport phenomena, microtubule-chromosome associations, and force transmission in nuclear division. Protoplasma. 1990;158:1-9.

72. Royou A, McCusker D, Kellogg DR, Sullivan W. Grapes (Chk1) prevents nuclear CDK1 activation by delaying cyclin B nuclear accumulation. J Cell Biol. 2008;183(1):63-75. pmid:18824564; PubMed Central PMCID: PMC2557043

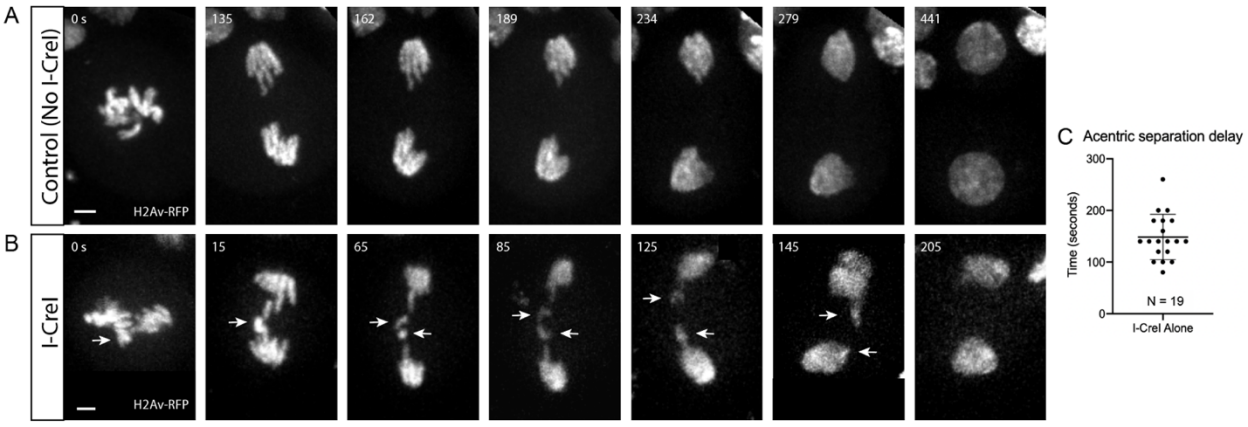
A
Control (No I-CreI)
0 s
135
162
189
234
279
441
H2Av-RFP
B
I-CreI
0 s
15
65
85
125
145
205
H2Av-RFP
C
Acentric separation delay
Time (seconds)
300
200
100
0
N = 19
I-CreI Alone

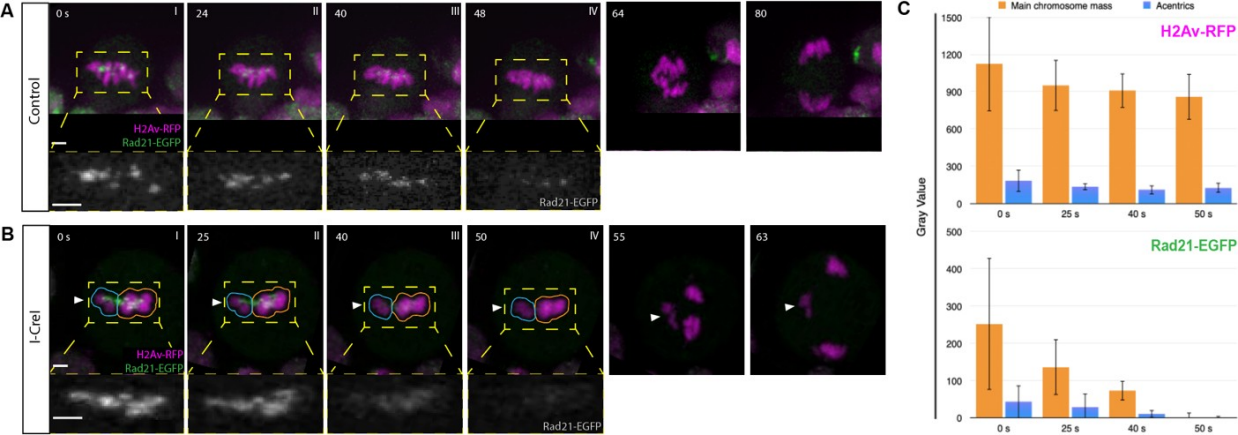
A
Control
0 s
I
24
II
40
III
48
IV
64
80
H2Av-RFP
Rad21-EGFP
Rad21-EGFP
B
I-CreI
0 s
I
25
II
40
III
50
IV
55
63
H2Av-RFP
Rad21-EGFP
Rad21-EGFP
C
Main chromosome mass
Acentrics
H2Av-RFP
Gray Value
1500
1200
900
600
300
0
0 s
25 s
40 s
50 s
Rad21-EGFP
500
400
300
200
100
0
0 s
25 s
40 s
50 s

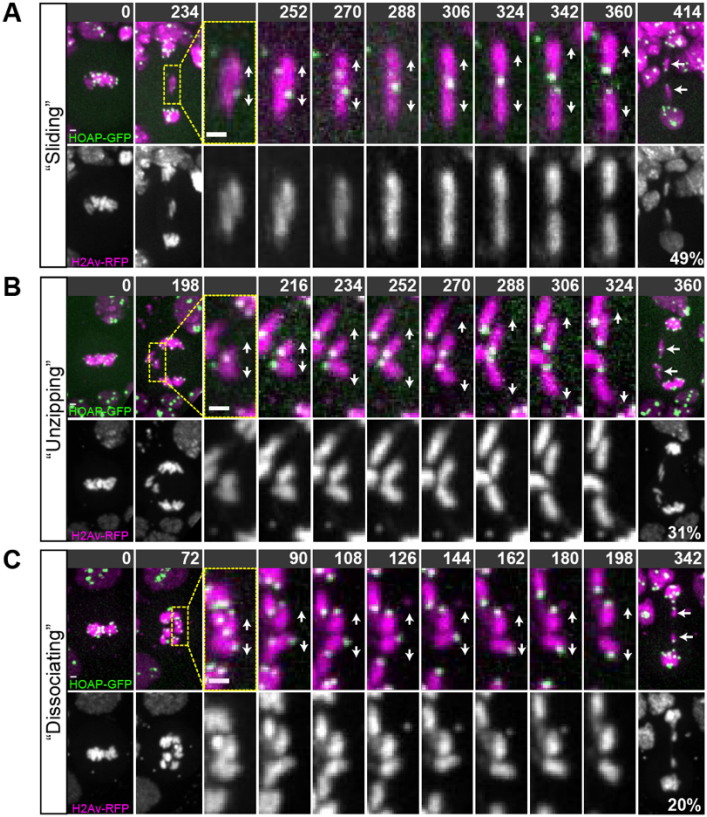

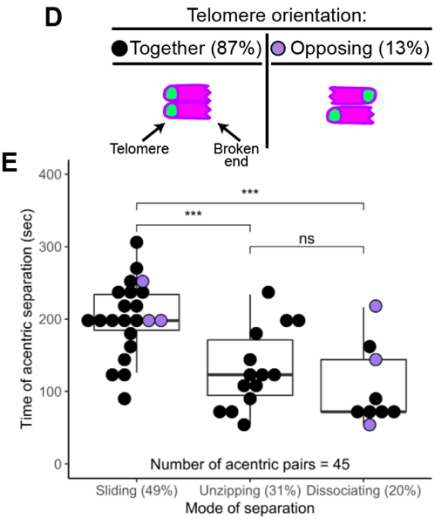

F

Mode of separation	Telomeres paired	Telomeres opposing	N =
Sliding	86%	14%	22
Unzipping	100%	0%	14
Dissociating	67%	33%	9

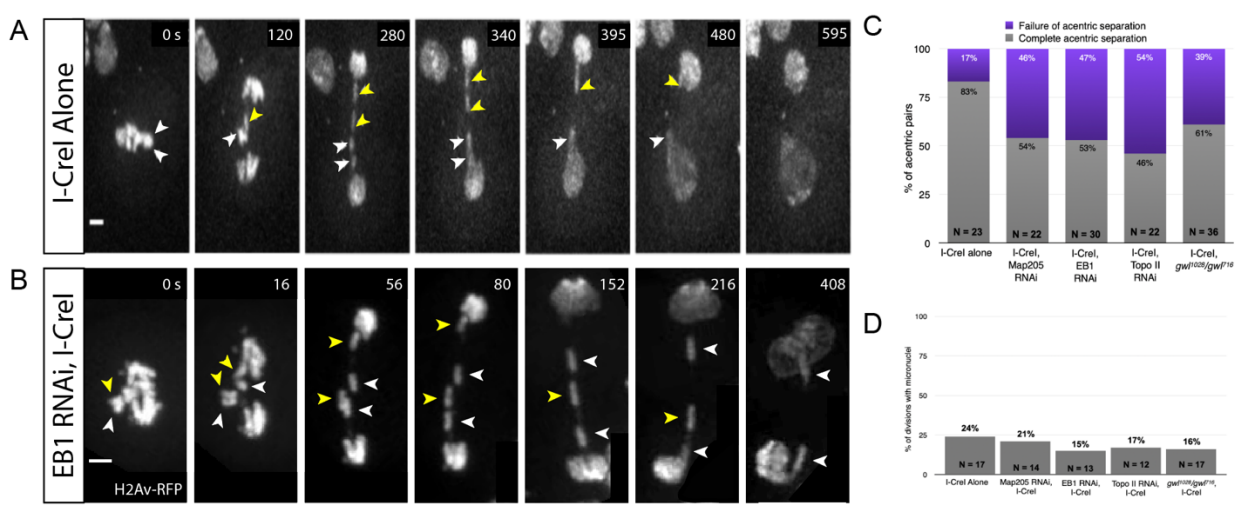
A
I-CreI Alone
0 s
120
280
340
395
480
595
B
EB1 RNAi, I-CreI
0 s
16
56
80
152
216
408
H2Av-RFP
C
Failure of acentric separation
Complete acentric separation
% of acentric pairs
100
75
50
25
0
17%
83%
46%
54%
47%
53%
54%
46%
39%
61%
N = 23
N = 22
N = 30
N = 22
N = 36
I-CreI alone
I-CreI, Map205 RNAi
I-CreI, EB1 RNAi
I-CreI, Topo II RNAi
I-CreI, gwl1028/gwlF16
D
% of divisions with micronuclei
100
75
50
25
0
24%
21%
15%
17%
16%
N = 17
N = 14
N = 13
N = 12
N = 17
I-CreI Alone
Map205 RNAi, I-CreI
EB1 RNAi, I-CreI
Topo II RNAi, I-CreI
gwl1028/gwlF16, I-CreI

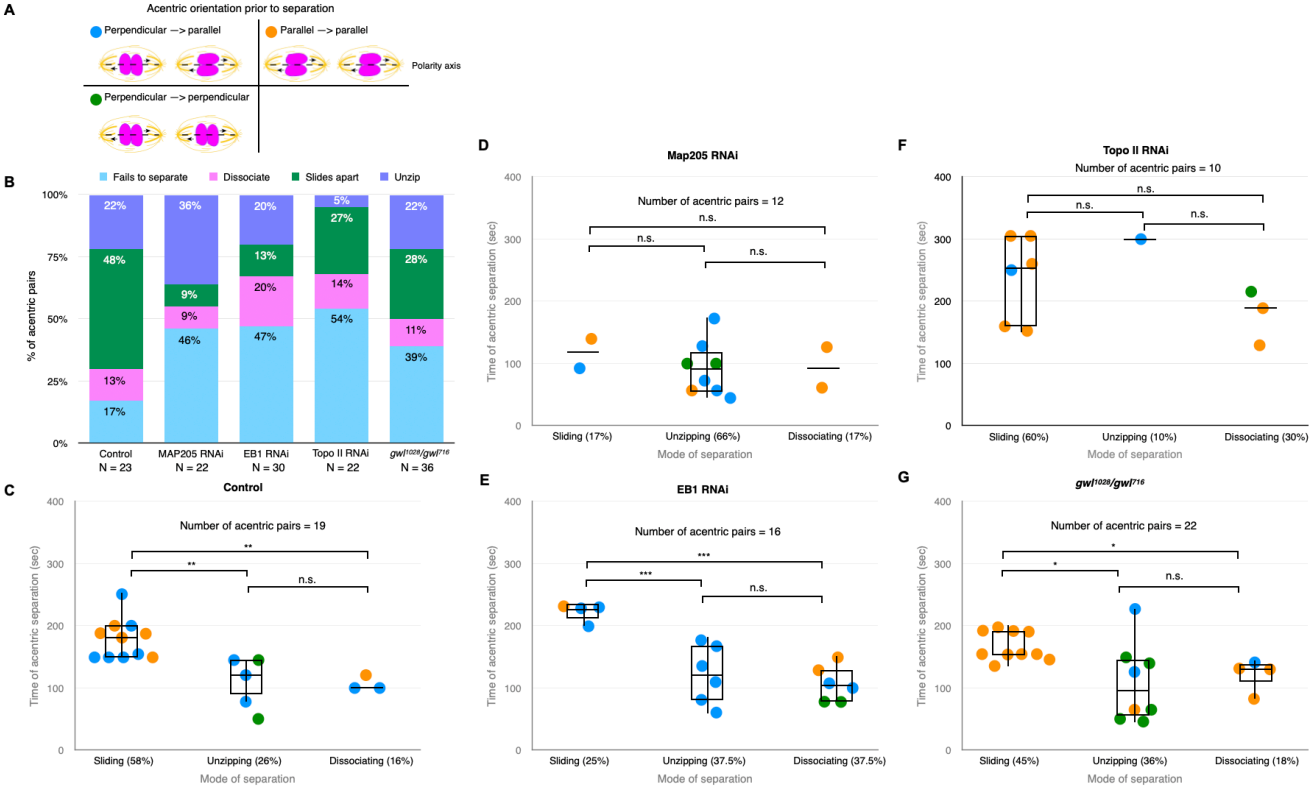
A
Acentric orientation prior to separation
Perpendicular —> parallel
Parallel —> parallel
Polarity axis
Perpendicular —> perpendicular
B
Fails to separate
Dissociate
Slides apart
Unzip
% of acentric pairs
100%
75%
50%
25%
0%
22%
48%
13%
17%
36%
9%
9%
46%
20%
13%
20%
47%
5%
27%
14%
54%
22%
28%
11%
39%
Control
N = 23
MAP205 RNAi
N = 22
EB1 RNAi
N = 30
Topo II RNAi
N = 22
gwl1028/gwlf16
N = 36
C
Control
Number of acentric pairs = 19
**
**
n.s.
Time of acentric separation (sec)
400
300
200
100
0
Sliding (58%)
Unzipping (26%)
Dissociating (16%)
Mode of separation
D
Map205 RNAi
Number of acentric pairs = 12
n.s.
n.s.
n.s.
Time of acentric separation (sec)
400
300
200
100
0
Sliding (17%)
Unzipping (66%)
Dissociating (17%)
Mode of separation
E
EB1 RNAi
Number of acentric pairs = 16
***
***
n.s.
Time of acentric separation (sec)
400
300
200
100
0
Sliding (25%)
Unzipping (37.5%)
Dissociating (37.5%)
Mode of separation
F
Topo II RNAi
Number of acentric pairs = 10
n.s.
n.s.
n.s.
Time of acentric separation (sec)
400
300
200
100
0
Sliding (60%)
Unzipping (10%)
Dissociating (30%)
Mode of separation
G
gwl1028/gwlf16
Number of acentric pairs = 22
*
*
n.s.
Time of acentric separation (sec)
400
300
200
100
0
Sliding (45%)
Unzipping (36%)
Dissociating (18%)
Mode of separation

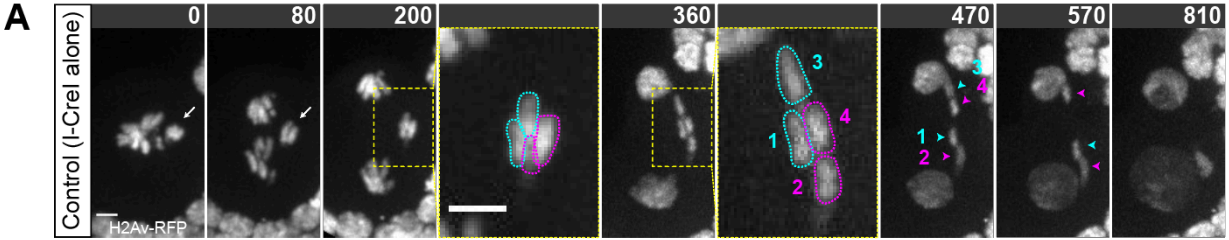
A
Control (I-CreI alone)
0
80
200
360
470
570
810
H2Av-RFP
1
2
3
4

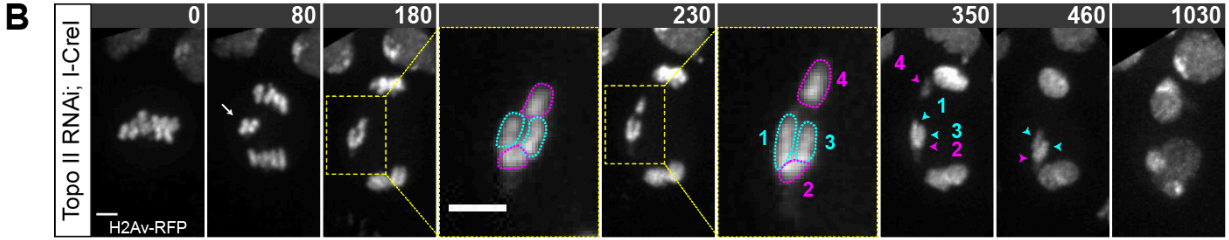
B
Topo II RNAi; I-CreI
0
80
180
230
350
460
1030
H2Av-RFP
1
2
3
4

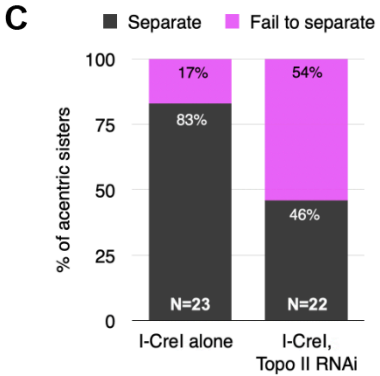
C
Separate
Fail to separate
% of acentric sisters
100
75
50
25
0
17%
83%
54%
46%
N=23
N=22
I-CreI alone
I-CreI, Topo II RNAi

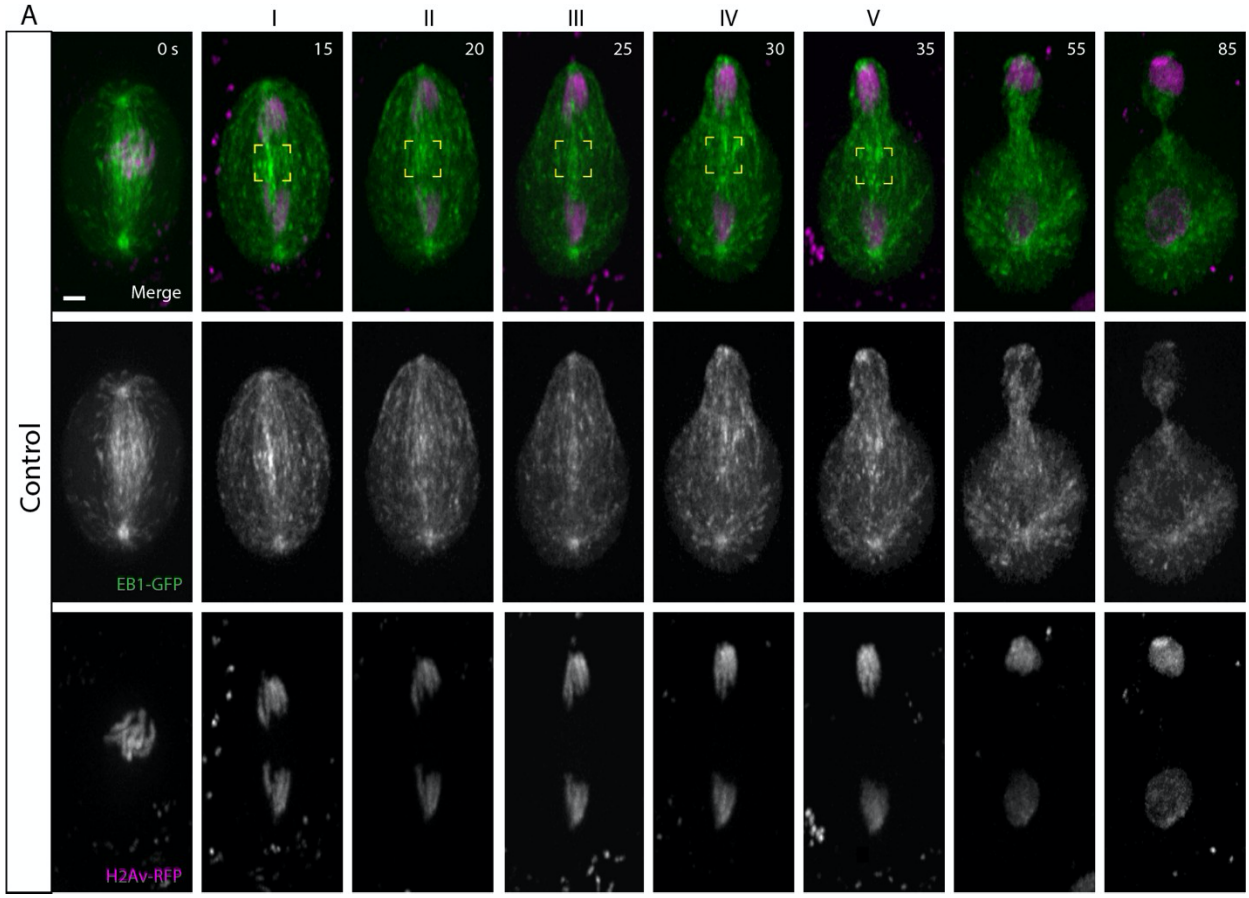
A
I
II
III
IV
V
Control
0 s
15
20
25
30
35
55
85
Merge
EB1-GFP
H2Av-RFP

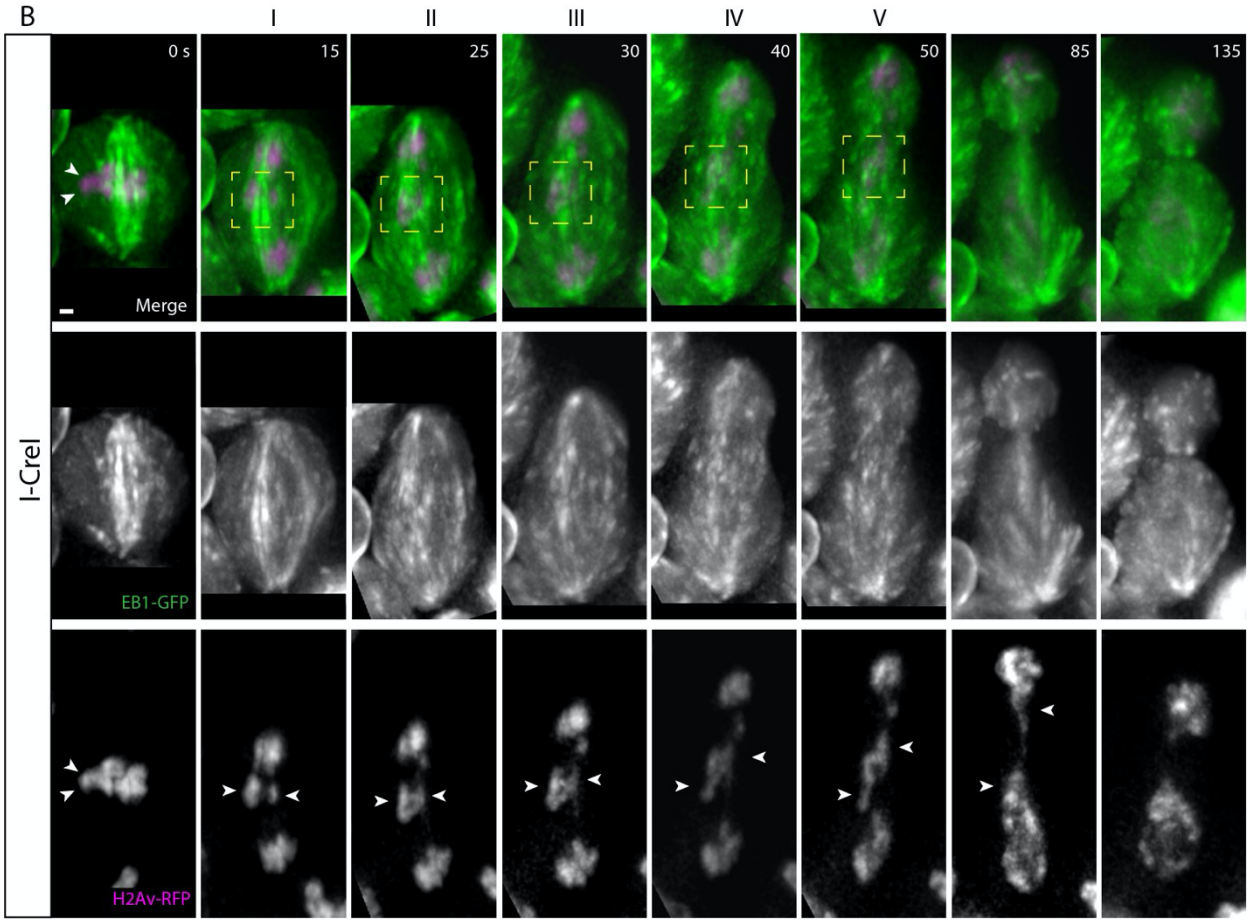
B
I
II
III
IV
V
I-Crel
0 s
15
25
30
40
50
85
135
Merge
EB1-GFP
H2Av-RFP

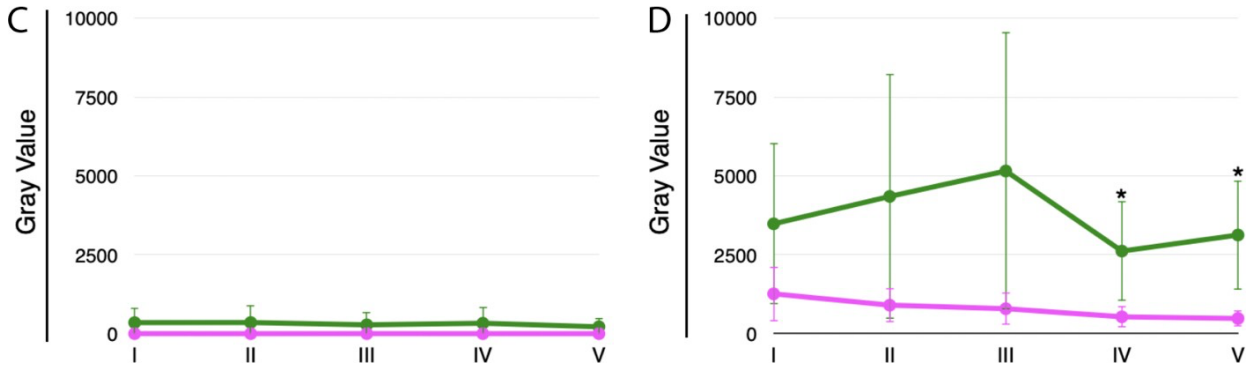
C
Gray Value
10000
7500
5000
2500
0
I
II
III
IV
V
D
Gray Value
10000
7500
5000
2500
0
*
*
I
II
III
IV
V

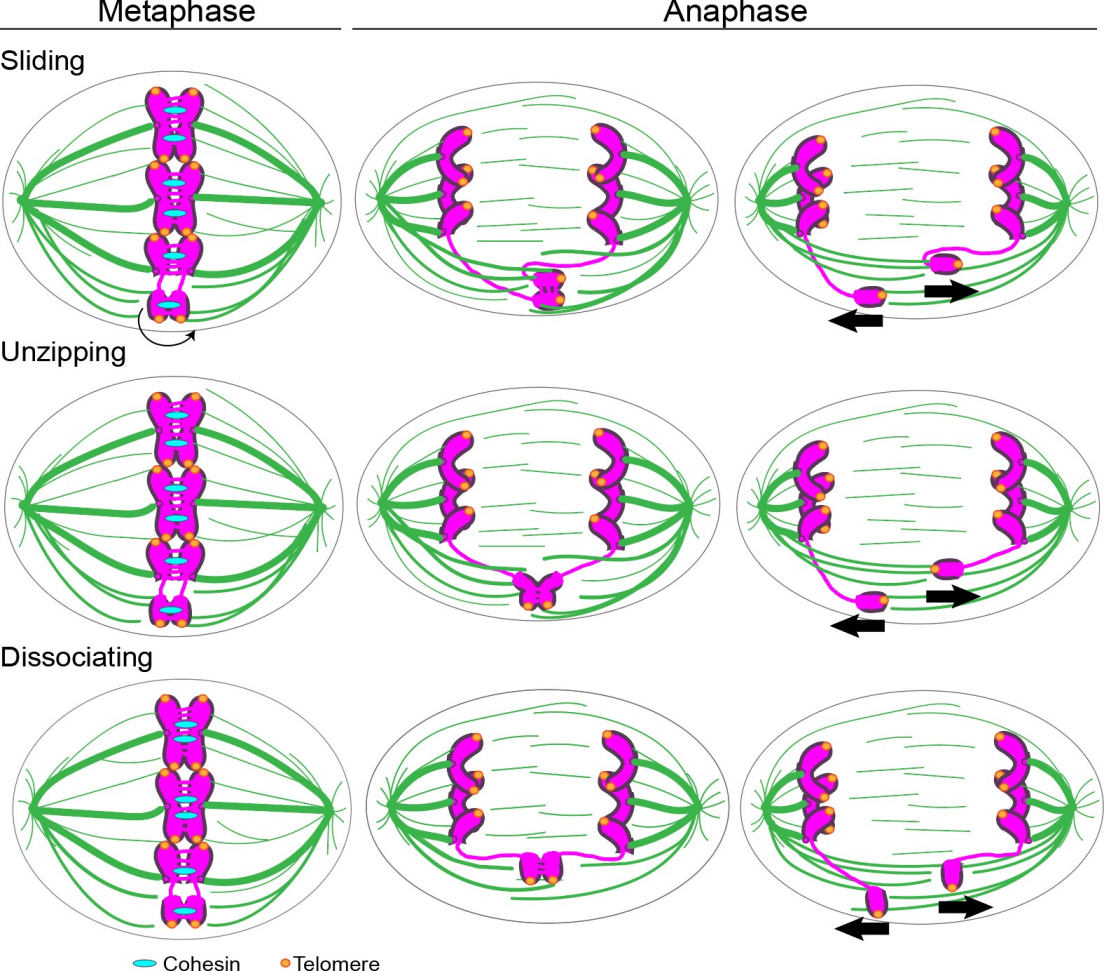
Metaphase
Anaphase
Sliding
Unzipping
Dissociating
Cohesin
Telomere